ADVANCED FUNCTIONAL MATERIALS
www.afm-journal.de

Photoexcited Polaron Relaxation as a Structurally Sensitive Reporter of Charge Trapping in a Conducting Polymer

*Abdul Rashid Umar, Austin L. Dorris, and Christopher Grieco**

Conjugated polymers (CPs) play a central role in electronic applications due to their easily tuned electronic and ionic conductivities via chemical or electrochemical doping. Although doping improves charge conduction by introducing high densities of carriers into the CP, the accompanying structural changes and their impact on carrier mobility remain elusive. Methods capable of probing carrier distributions and their dependence on polymer morphology are needed to better understand how to improve conductivity. Here, a transient absorption (TA) spectroscopy approach is demonstrated, capable of directly probing mobile and trapped carriers in doped CPs and that is also sensitive to polymer nanostructure by using a model polythiophene system with tuned crystallinity. Exciting polarons in the polymer films produces distinct photoinduced absorption signals in the near-infrared spectrum that decay during the picosecond timescale in the form of biphasic, stretched exponential kinetics, which reflect a distribution of mobile (free) and trapped polarons. The kinetic analysis provides evidence for mobile polarons irrespective of polymer film crystallinity, whereas polarons located in impure amorphous phases with reduced chain ordering exist within a deeper distribution of trap states. Altogether, these observations suggest a stronger correlation of carrier trapping with local chain ordering (planarity or aggregation) rather than polymer crystallinity.

1. Introduction

Interest in conjugated polymers (CPs) for electronic applications continues to increase due to their commercial availability, synthetic accessibility, and solution processability.[1–5] The chemical and redox tunability of CPs makes it possible to engineer conducting materials with varying optical properties, structure, and morphology.[1] CPs facilitate charge transport via π-electron delocalization and interchain coupling, and incorporation of hydrophilic side chains additionally imparts the ability to conduct ions in aqueous environments,[6,7] expanding their utility in bioelectronic and energy storage devices.[8–11] However, conductivity is known to be sensitive to the structure and morphology of CPs but in elusive ways,[7,12] warranting deeper investigation into their structure-function relationships.[13]

Chemical doping is an effective method for converting CPs to their conductive forms, whereby a redox agent introduces permanent charges within the polymer backbone to increase the charge density and conductivity.[14–16] In the case of p-type doping (oxidation), a positive charge carrier (hole polaron) is introduced into the polymer, leaving behind a electrostatically-stabilizing counterion (reduced dopant).[17–21] This Coulombic hole-ion interaction, in addition to morphological changes that accompany the doping process, impact the conductivity of the CP[22–24] in complex ways. For example, many studies[25–28] attribute the generation of mobile carriers and improved conductivity to CPs with higher crystallinity, while other reports[29–32] disagree. New approaches that are sensitive to both the amorphous and crystalline phases of CPs, and that can be used to probe the full distribution of mobile and trapped polarons, are needed for refining these structure-property relationships.

Recent works from our group and the Schwartz group have demonstrated transient absorption (TA) spectroscopy, in which polarons are directly photoexcited, as a promising technique for strategically probing their electronic properties directly.[33,34] For example, we showed how the photoinduced Stark effect that is produced via polaron photoexcitation in TA spectroscopy measurements can be used as a sensor of the nanoscale structural and electronic environments of hole polarons in a doped 3,4-propylenedioxythiophene-co-3,4-ethylenedioxythiophene (ProDOT-*co*-EDOT) polymer film.[33] In a pioneering study, Voss et al. showed how the ultrafast relaxation dynamics of photoexcited polarons can be used to distinguish between trapped (coulombically bound) and free (less coulombically bound) polarons in a chemically doped poly(3-hexylthiophene-2,5-diyl) (P3HT) polymer film.[34] These encouraging findings suggest that TA spectroscopy can be further developed and applied to elucidate relationships between polymer film nanomorphology and the corresponding populations of trapped and free polarons.

In this study, we use TA spectroscopy to investigate the effect of polymer film crystallinity and morphology on the trapping of chemically induced charge carriers by exploiting

A. R. Umar, A. L. Dorris, C. Grieco
Department of Chemistry and Biochemistry
Auburn University
Auburn, AL 36849, USA
E-mail: czg0090@auburn.edu

The ORCID identification number(s) for the author(s) of this article can be found under https://doi.org/10.1002/adfm.202407181

DOI: 10.1002/adfm.202407181

their ultrafast excited state relaxation dynamics. Two chemically doped model polymer films containing regioregular poly(3-hexylthiophene) (P3HT) are compared: A pure, nanocrystalline P3HT film and an amorphous blend film containing a mixture of P3HT and poly(9,9-dioctylfluorene-alt-benzothiadiazole) (F8BT). F8BT was chosen because it is known to prevent P3HT crystallization due to their high miscibility,[35] and it is an electronically intert additive that cannot be chemically oxidized even with strong oxidants like magic blue (tris(4-bromophenyl)ammoniumyl hexachloroantimonate).[36]

Absorbance spectrophotometry and grazing-incidence X-ray diffraction (GI-XRD) are used to study structural changes in the films before and after chemical doping with $Fe(ClO_4)_3$, and confirmed that the pure P3HT film contained nanocrystalline 2D lamellae, while the P3HT:F8BT blend film was amorphous and contained weakly interacting P3HT aggregates. Photoexciting hole polarons in P3HT using 0.62 eV (2000 nm) light led to two key features in the 0.53–2.48 eV (500–2350 nm) TA spectra: First, an electroabsorption (EA) signal arising from the photoinduced Stark effect confirmed that polarons in the pure P3HT film reside in the lamellar phase. Second, the decay kinetics of a near-infrared photoinduced absorption (PIA) signal revealed that both films contain similar populations of mobile and trapped polarons, despite significant differences in their crystallinities. Kinetic modeling results suggest that local polymer chain ordering, but not necessarily crystallization, is required for the formation of mobile polarons in chemically doped polymers. Our TA spectroscopy results highlight how photoexcited polaron relaxation dynamics can reveal information about the distribution of free and trapped polarons in CPs.

2. Results and Discussion

2.1. Polymer Film Nanostructure and Polaronic Transitions

A combination of absorption spectroscopy and grazing incidence X-ray diffraction (GI-XRD) was used to characterize the morphology of two thin films fabricated using polymer blends with different ratios of P3HT and F8BT polymers. Ultrafast transient absorption (TA) spectroscopy was then used to probe the influence of polymer film morphology on the nature and behavior of the chemically induced charge carriers. The molecular structures of the polymeric materials studied (i.e., P3HT and F8BT) are shown in **Scheme 1**. Herein, the polymer film cast from a pure regioregular P3HT solution will be referred to as the (100:0) polymer film, while that from the P3HT:F8BT solution will be referred to as the (50:50) polymer film. P3HT is known to form a periodic 2D lamellar structure, which enhances its ordering and crystallinity.[1,37] Several studies have evidenced large miscibility between P3HT and F8BT, making it possible to fabricate electron donor–acceptor blends, although F8BT hinders P3HT crystallization.[35,38–41] Thus, the (100:0) and (50:50) polymer films are expected to contain ordered nanocrystallites and disordered, mixed polymer phases, respectively, making it possible to probe the influence of nanomorphology on charge carrier properties. Note that despite the large miscibility of P3HT and F8BT, some molecular-level phase separation is expected due to narcissistic self-sorting, preventing uniform mixing. Since F8BT is an n-type semiconductor with a deep valence band, $Fe(ClO_4)_3$ is expected to selectively oxidize (dope) only the P3HT chains in the polymer blend.[36]

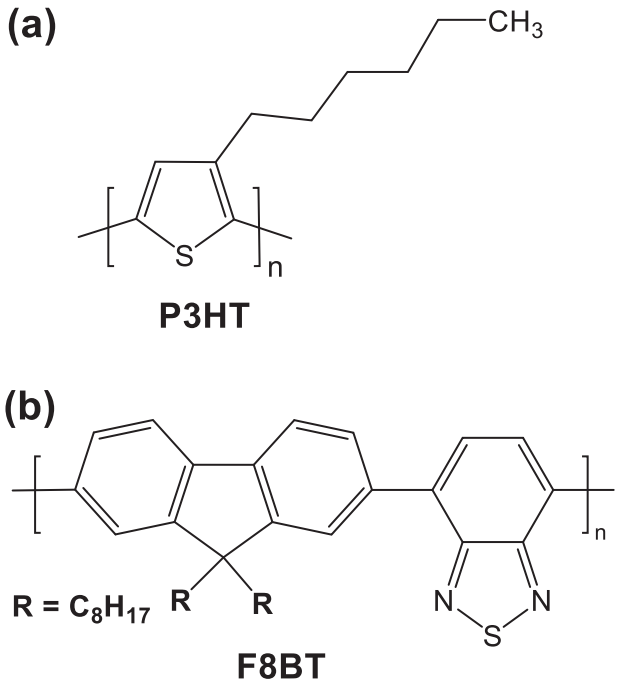

Scheme 1. Molecular structure of a) poly(3-hexylthiophene-2,5-diyl) (P3HT) and b) poly(9,9-dioctylfluorene-alt-benzothiadiazole) (F8BT).

The steady-state absorption spectrum of each undoped polymer film, which shows only a bandgap (BG) absorption band above 1.90 eV, confirms that F8BT prevents ordering of the P3HT chains (compare bright red and bright blue curves in **Figure 1a**). The BG absorption band of the pure, undoped F8BT polymer film (0:100) is centered at ≈2.68 eV, and that for the undoped (100:0) polymer film is centered at ≈2.32 eV. The characteristic vibronic structure of the BG band of the (100:0) polymer film reflects planarization and aggregation of P3HT chains as seen in 2D lamellae.[1,42–44] However, the undoped (50:50) polymer film shows a blueshifted and less structured BG band with an onset at ≈2 eV and peaking between 2.2 and 2.7 eV (bright blue curve in Figure 1a), which reflects disordered P3HT chains.[45]

GI-XRD measurements on the polymer films were performed to study differences in their crystallinities. The GI-XRD pattern of the undoped (100:0) polymer film shows an intense lamellar spacing peak (100) at 0.38 $Å^{-1}$ and a weak 2nd order peak at ≈0.76 $Å^{-1}$ (**Figure 2**). While the (010) peak could not be detected in our 1-D, in-plane GI-XRD measurements, the presence of the (100) peak, along with the vibronic structure seen in the absorption spectrum in Figure 1a, strongly suggests that the P3HT chains π-stack to form 2D lamellae.[1] On the other hand, the (50:50) polymer film lacks clear diffraction features, indicating that F8BT prevents the P3HT chains from crystallizing, rendering the film highly amorphous (see Figure 2).[1] The XRD pattern of an undoped F8BT film (see Figure S1, Supporting Information) shows no indication of crystallites, indicating that this polymer is inherently amorphous. Note that despite the highly ordered nature of P3HT, it is semicrystalline and so the (100:0) polymer film is expected to also contain some fraction of amorphous phase.[46,47]

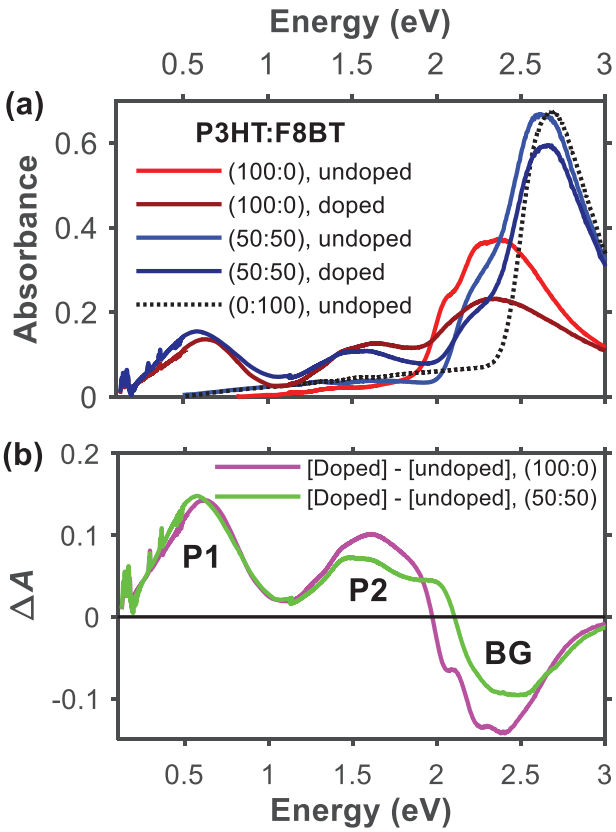

Figure 1. a) Steady-state absorption spectra of undoped and doped polymer films of P3HT (red and dark red) and P3HT:F8BT polymer blend (blue and dark blue), and undoped F8BT (black, dotted) on CaF_2 substrates. The polymer films were sequentially doped with an n-butyl acetate solution containing 0.05 mg mL^{-1} $Fe(ClO_4)_3$. b) Absorbance difference between the spectra of the doped polymer films and their corresponding undoped films.

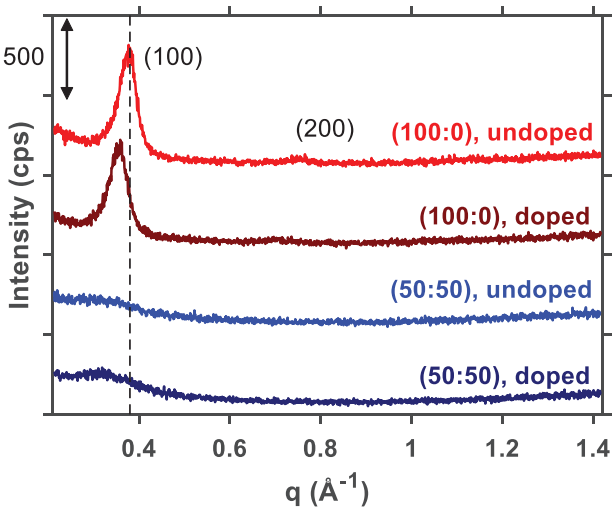

Figure 2. Grazing incidence X-ray diffraction (GI-XRD) of undoped (red) and doped (dark red) P3HT:F8BT (100:0) polymer film, and undoped (blue) and doped (dark blue) P3HT:F8BT (50:50) polymer film on glass substrates.

Characteristic optical features of doped CPs are observed upon treating the polymer films with n-butyl acetate solutions containing 0.05 mg mL^{-1} $Fe(ClO_4)_3$. This doping process decreases the BG absorption while simultaneously introducing the P1 and P2 polaronic bands in the near-infrared (near-IR) for both the (100:0) and (50:50) films (see Figure 1a,b). Attempts to chemically oxidize a pure F8BT film with $Fe(ClO_4)_3$ were not successful, as expected due to its deep-lying HOMO level.[36] Therefore, the charge carriers in the doped (50:50) polymer film form via oxidation of only the P3HT chains. We attempted to achieve similar doping levels between the two films by adjusting the doping time until the fractional decrease in the BG absorption band for each film was close. From the data in Figure 1a, the 100:0 film had a decrease in BG peak area of ≈0.73 while that of the 50:50 film was 0.88. Despite these minor variations, we found that the transient absorption kinetic data were not dependent on doping level in either film (vida infra).

The doping times necessary to reach similar P1 and P2 band intensities for the (100:0) and (50:50) films reveal further insights into the dependence of doping efficiency on polymer nanostructure. Half the dopant exposure time was needed for the (100:0) film, suggesting that the highly ordered polymer chains oxidize more efficiently. This observation is consistent with reports of higher energetic driving force for doping crystalline regions compared to amorphous domains in P3HT.[48]

The absorption difference spectra between doped and undoped films in Figure 1b reveal clearer insights into the doping process. The reduction of vibronic features in the BG band of the (100:0) polymer film in the 2–2.5 eV region indicates that the dopant perturbs the lamellar structure of the nanocrystallites. This observation, combined with the shift of the (100) diffraction peak to lower *q* upon doping (Figure 2), indicates dopant-induced expansion of the crystalline lattice. These changes correspond to an increase in the lamellar d-spacing from ≈1.66 to 1.75 nm. A control experiment shows that the n-butyl acetate solvent used in the doping process is not responsible for this lattice expansion itself (Figure S1, Supporting Information), suggesting that at least some of the dopant molecules intercalate the P3HT lamellae.

The lack of vibronic structure in the negative BG band for the (50:50) film confirms that the amorphous (i.e., non-crystalline) regions of P3HT are also oxidized under the doping conditions used, despite the expected lower energetic driving force. The GI-XRD pattern of the doped (50:50) film in Figure 2 shows a weak and broad feature near 0.33 $Å^{-1}$, suggesting that the dopant may induce aggregation (and hence local ordering) of the P3HT chains in amorphous regions. Unlike in pure, undoped regiorandom P3HT films that contain highly disordered, nonplanar chains, the regioregular P3HT chains in the (50:50) blend film exhibit local ordering, suggesting that there is some phase separation on the molecular scale (see Supporting Information). In particular, Figure S2 (Supporting Information) shows that the isolated absorption spectrum of the P3HT phase within the P3HT:F8BT mixture shows a BG peak centered near 2.5 eV, which is redder than that of a pure undoped regiorandom P3HT film (2.75 eV). This observation suggests that the average conjugation length of the P3HT in the (50:50) blend film is greater than that of highly disordered regiorandom P3HT. Furthermore, this finding is consistent with the appearance of a negative band at ≈2.4 eV in the absorbance difference spectrum of the (50:50) film

in Figure 1b. The additional appearance of slight vibronic structure in Figure S2b (Supporting Information) suggests that P3HT chains in the (50:50) blend film form small aggregates. Note that the absorbance difference spectrum for the doped (50:50) polymer film shows no negative band centered near 2.6 eV (green trace in Figure 1b), confirming that the $Fe(ClO_4)_3$ dopant does not oxidize the F8BT chains, as expected.[36] Altogether, we conclude that the P3HT domains in the (50:50) blend film are non-crystalline but contain small aggregates of P3HT chains.

The positive signals in the absorption difference spectra in Figure 1b provide details on the electronic nature of the polarons. The spectra of the doped (100:0) and (50:50) films both show P1 bands with similar shapes and peak positions. Several studies[18,19,23,28,49] have shown how the P1 absorption band position depends on the polymer morphology and polaron-ion Coulombic interactions within the CP film. For example, Scholes and co-workers have correlated a redshift of the P1 absorption band in a chemically doped P3HT film to an increase in the crystallinity, where polaron delocalization is expected to increase.[19,28] Ghosh et al. also calculated a P1 absorption redshift by increasing the distance between the polaron and its counter-anion, which reduces the polaron-ion Coulombic interaction.[23] Even though the oxidation of the (100:0) polymer creates polarons in both the ordered and amorphous regions, the close agreement between the P1 bands in the doped (100:0) and (50:50) film spectra suggests that the chemically induced polarons in both films are localized to single chains.

The P1 peak position for both the sequentially doped (100:0) and (50:50) polymer films is seen at ≈0.55 eV (see Figure 1b), which is expected for P3HT films sequentially doped using an orthogonal solvent.[50] Both experiment[29,51] and theory[23] show that a hole polaron localized on a single polymer chain, which is expected to readily occur in amorphous phases, has a relatively high-energy P1 transition energy. In sequential doping, the oxidant is reported to more easily access disordered regions in P3HT films because the dopant solution primarily swells the amorphous phase.[52] However, the shift of the lamellar spacing to lower q in the doped (100:0) polymer film, as observed in Figure 2, suggests that the dopant molecule also has access to the ordered region of the (100:0) polymer film.[28] This may lead to the generation of polarons that delocalize across multiple chains (2D polarons) in the ordered region. 2D polarons are expected to have a peak at 0.06 eV, as seen in a photoinduced absorption (PIA) study of undoped regioregular P3HT following exciton excitation;[53] however, we do not observe this signal in the absorption spectrum of the (100:0) polymer film (Figure 1). Therefore, the relatively high-energy P1 transition energy in the doped (100:0) polymer film suggests that polarons in the crystalline regions do not delocalize across multiple chains in this film (i.e., they are 1D polarons).

Polarons are also expected to form in amorphous domains in both the (100:0) and (50:50) films. The relatively high-energy P1 transition energy of the doped (100:0) film, reduction of vibronic features in the BG band (Figure 1), and the shift of the (100) diffraction peak to lower q upon doping (Figure 2) signify the doping of both the ordered and amorphous regions in the (100:0) polymer film. The presence of the counter-ion, however, prevents the polarons in the ordered region from exhibiting 2D polaron characteristics. The lack of clear diffraction features in the (50:50) polymer film (Figure 2) signifies that polarons must form in disordered (non-crystalline) regions in this film.

The extra peak near 2.02 eV in the difference spectrum of the doped (50:50) film is tentatively assigned to the P3 (and P3') polaronic transition (see green trace in Figure 1b). While the P3 and P3' transitions in doped CPs are strictly symmetry-forbidden according to electronic structure calculations,[54] disorder in the polymer chains and interchain delocalization of the polaron are both believed to increase its oscillator strength.[34] According to the traditional electronic model for polarons in CPs, the energy of the P3 transition (E_{P3}) should equal the sum of the P1 and P2 transition energies (E_{P2} + E_{P1}). From Figure 1b, a value of E_{P3} = 2.07 eV is predicted using E_{P1} = 0.57 eV and E_{P2} = 1.50 eV, which matches the position of the extra peak. Furthermore, our transient absorption measurement of a regiorandom P3HT:PC_{61}BM blend film (Figure S3, Supporting Information), which shows a photogenerated polaron absorption spectrum that qualitatively resembles that of the chemically doped (50:50) film, additionally supports this P3 peak assignment.

2.2. Ultrafast Photoexcited Polaron Dynamics

Figure 3 represents the transient absorption (TA) results for the doped (100:0) and (50:50) films, which were excited at the P1 transition at 0.62 eV (2000 nm) and detected in the 0.53–2.48 eV (500–2350 nm) spectral window. Within 200 fs of excitation, three negative transient signals appear near 2.3 eV (540 nm), 1.67 eV (743 nm), and 0.65 eV (1900 nm) (see Figure 3a,b). Additionally, small positive peaks are seen near 1.97 eV (629 nm) for the doped (100:0) polymer film and 2.04 eV (609 nm) for the doped (50:50) polymer film, while an intense peak appears at ≈1.24 eV (1000 nm) for both polymer films (see Figure 3a,b). In a previous report on chemically doped P3HT films by Voss et al., the negative band at 1.7 eV was assigned to the P3 bleach while the positive band at ≈1.25 eV was assigned to a induced P2 absorption when photoexciting the P1 transition.[34] In our TA spectra, which are recorded over a wider spectral region, the negative band near 0.7 eV is assigned to the P1 bleach.

Although both doped polymer films produce qualitatively similar transient spectra, they contain some features that depend on P3HT morphology. For the doped crystalline (100:0) polymer film, the negative band in the visible region centered at 2.26 eV (549 nm) has clear vibronic features (Figure 3a). However, for the doped amorphous (50:50) polymer film, the negative band at 2.31 eV (537 nm) lacks vibronic features (Figure 3b). Although the absorbance difference spectrum of the (100:0) film in Figure 1b (pink curve) shows that the dopant perturbs the ordering of the P3HT chains, as generally seen for sequential chemical doping,[36,55,56] the observation of vibronic features in the corresponding TA spectrum indicates that the photoexcited polarons must still be located within or near ordered phases in the (100:0) film, which includes both crystalline and amorphous domains. The lack of vibronic features in the doped (50:50) polymer film indicates that the photoexcited polarons reside in disordered phases in this film, which is consistent with the absence of crystalline domains in the blend film deduced from the steady-state absorption spectra in Figure 1.

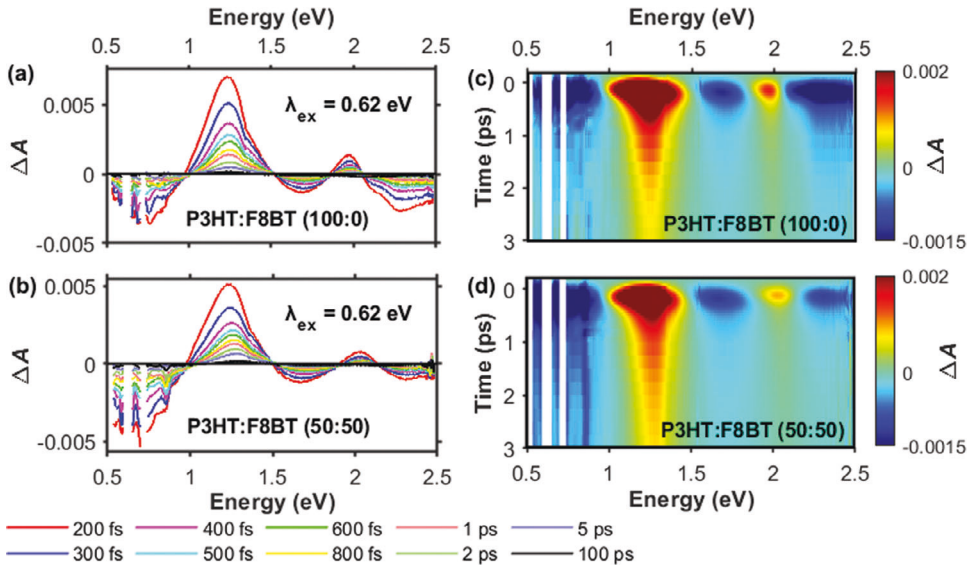

Figure 3. Ultrafast Vis-NIR transient absorption spectra with 0.62 eV (2000 nm) excitation recorded at a series of time delays for chemically doped CP films fabricated from a) P3HT solution (100:0) and b) P3HT:F8BT polymer blend (50:50) in the 0.53–2.48 eV region. The excitation fluence was 160 and 132 μJ cm^{-2}, respectively. 2D maps of the transient absorption spectra of the c) (100:0) polymer film and d) (50:50) polymer film.

The derivative-like feature ("EA signal") in the TA data within the 1.82–2.47 eV region is due to photoseparation of the hole polaron from its counter-anion, which induces a Stark effect on the P3HT BG transition.[33] This photoinduced charge separation process generates a local electric field that shifts the BG transition energy of nearby neutral chains. **Figure 4** provides a closer view of the EA signals identified in Figure 3 at 200 fs, which is our earliest resolvable time delay. The EA signal of the doped (100:0) polymer film is approximately twice as intense as that of the doped (50:50) polymer film. The magnitude of an EA signal is known to track with electric field strength.[57,58] Therefore, the more intense EA signal for the (100:0) film suggests that a stronger electric field is produced on average as the hole polaron separates from the counter-anion because many of the polarons reside in ordered P3HT domains. The position of the EA signal, which appears to be redshifted by ≈0.07 eV for the doped (100:0) polymer film (compare the zero-crossings and the red and blue dashed lines in Figure 4), indicates that the transient field at 200 fs perturbs lower-energy BG transitions on average in the (100:0) film, which is expected for this sample because its polarons reside in or near ordered domains. Altogether, these observations indicate that the ordering of P3HT chains in the (100:0) film, which supports intrachain polaron delocalization, enables larger polaron-ion photoseparation distances. Note that the appearance of the P1 band at ≈0.5 eV in the steady-state absorbance spectrum of the (100:0) film (Figure 1) signifies the localization of polarons to single chains, but this cannot alone differentiate whether these polarons reside in crystalline or amorphous regions. However, the EA signal in transient absorption spectroscopy is able to provide more detailed information on polaron environment.

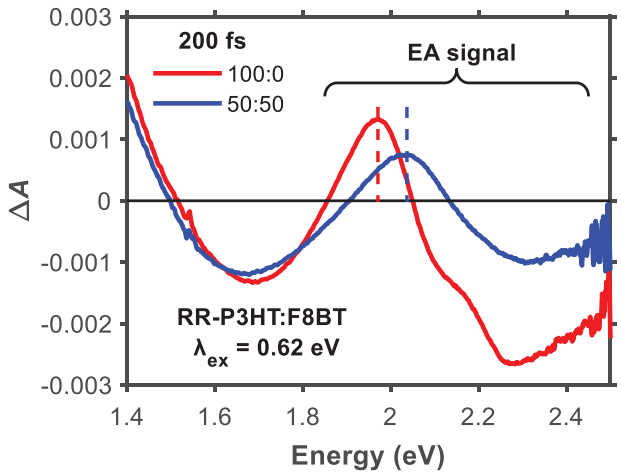

Figure 4. TA spectra at 200 fs time delay for the doped (100:0) polymer film (red) and (50:50) polymer film (blue) with spectra range of 1.4–2.48 eV. The dashed vertical red and blue lines highlight the relative shift of the positive portion of the electroabsorption (EA) signal. The initial excited state density was controlled in the experiment so that the relative intensities between the two traces could be compared. Note that the location of the EA signal is indicated by the curly brackets, however, the negative-going part of the spectra also contains overlapping ground-state bleach signals.

We next considered whether the transient field produced in the (50:50) film by ion-hole photoseparation in the P3HT phase can also induce a Stark shift of nearby F8BT chains. Given the steep linear absorption band of F8BT (Figure 1a), a Stark shift is expected to produce a large EA signal below ≈2.5 eV, which would interfere with that of P3HT; however, Figure 4 does not exhibit such a feature. Therefore, we conclude that the F8BT and P3HT chains are not uniformly mixed, suggesting that the two polymers are phase-separated on the molecular level.

In addition to providing spectral information, TA spectroscopy reveals dynamical information about the excited carriers. The photoinduced absorption (PIA) band centered at ≈1.24 eV (see Figure 3) appears to blueshift during the measured timescale for both polymer films, which suggests the presence of overlapping

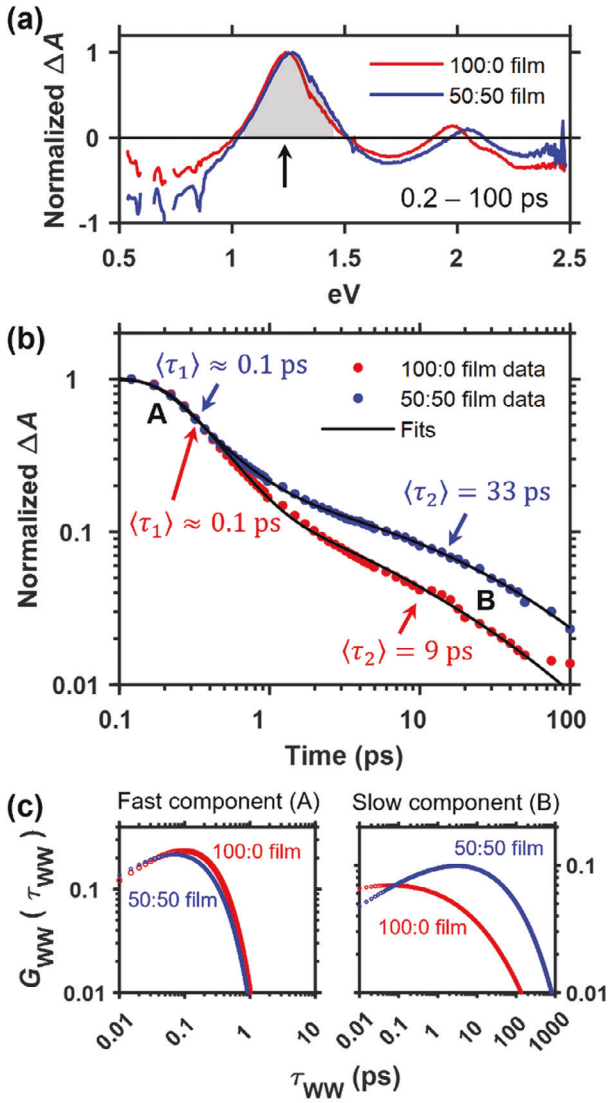

Figure 5. a) Transient absorption spectra averaged over 0.2–100 ps for the 100:0 and 50:50 films. The gray shaded area highlights the part of each spectrum that was averaged to obtain the decay kinetics in (b). b) Normalized peak area kinetics of the near-IR PIA band at ≈1.24 eV for the doped (100:0) and (50:50) polymer films. The black curves are fits to the kinetic data using a sum of two stretched exponential functions. The labels "A" and "B" point out the fast and slow decay components in the kinetic traces. The average time constants are indicated for each component for each film. c) Plots of the relaxation time distribution function (Williams–Watts distribution, WW) against time constant for the fast (left) and slow (right) kinetic decay components for each film.

peaks with different decay kinetics. To fully capture these dynamics, we monitored the peak area kinetics for the doped polymer films (see **Figure 5**), which revealed two key results. First, each kinetic trace in Figure 5b shows biphasic decay over 0.1–100 picoseconds with a fast decay component (labeled "A") and a slow decay component (labeled "B"). Second, the slow kinetic decay component appears to decrease in signal intensity more slowly for the (50:50) film. Varying the doping level of the polymer films resulted in similar observations, with no dependence of the normalized kinetic decays on doping level (Figure S4, Supporting Information). As we will discuss below, these features provide details on the differences in Coulombic and structural environments of the polarons and reveal that crystallization is not a requirement for supporting mobile polarons in chemically doped P3HT films.

In a similar experiment, Voss et al. reported biexponential TA decay kinetics of a near-IR PIA band in a P3HT film chemically doped with 2,3,5,6-tetrafluoro-7,7,8,8-tetracyanoquinodimethane (F4TCNQ) and excited at the high-energy side of the P1 band.[34] The authors attributed the fast and slow decay components of the PIA band to the relaxation of less coulombically bound ("free") and more coulombically bound ("trapped") polarons, respectively, as they diffuse back to the counterions. Their assignment is based in part on the expectation that free polarons form in more ordered regions of the polymer where they can diffuse more rapidly.[34] Based on the consistency of our decay kinetics with those reported by Voss et al.,[34] we therefore attribute the fast and slow decay components observed in our TA experiment to mobile (Coulombically-free) and trapped polarons, respectively.

Surprisingly, the fast decay component (region "A" in Figure 5b) appears qualitatively similar in decay time and relative amplitude for both the doped (100:0) and (50:50) polymer films despite the significant difference in their morphology. This observation indicates that mobile (Coulombically-free) polarons form in the doped (50:50) polymer film despite the lack of crystalline P3HT domains. The result further suggests that the formation of mobile (free) polarons does not require the doping of extended 2D lamellar phases. Note that although our time resolution is ≈0.25 ps (see Section S5.2, Supporting Information), we estimate the average time constants obtained from our convolution fits to be on the order of ≈0.1 ps. While the limited time resolution also prevents us from precisely quantifying the ratios of the fast versus slow decay components, the qualitative appearance of a fast decay component in the kinetics of the (50:50) film allows us to conclude that mobile polarons do form in this film.

Our observation of mobile polarons in the amorphous P3HT:F8BT film from the TA kinetics supports recent works showing that doped amorphous polymer domains can counterintuitively improve charge conductivity.[50,59,60] For example, a sequentially doped polymer film containing 50% regioregular (RR) P3HT and 50% regiorandom (RRa) P3HT was demonstrated to have a four-fold higher conductivity than that of a doped polymer film containing 100% RR-P3HT.[29] Another study also demonstrated the generation of high carrier mobilities in a chemically doped P3HT film despite significant loss of polymer crystallinity induced by a large dodecaborane-based dopant molecule.[61]

We next considered possible mechanisms for the formation of mobile polarons in our films. In a recent report on regioregular P3HT, Zhong et al. suggested that doping the interfacial sites between the nanocrystalline (lamellar) and amorphous phases increases polaron mobility because the counter-anion becomes spatially trapped in the amorphous phase while the polaron diffuses away into the ordered phase and decreases their Coulombic interaction.[55] However, our TA analysis of the (50:50) film indicates that extended, crystalline lamellar phases are not required for forming mobile polarons. The weak and broad diffraction feature near 0.33 $Å^{-1}$ in GI-XRD pattern of the doped (50:50) film (see dark blue trace in Figure 2) indicates that the

dopant induces local ordering of P3HT chains in amorphous domains. Therefore, we conclude that dopant-induced aggregation[45] or planarization[29,62] of the P3HT chains underlies the formation of mobile polarons. While additional work is needed, we propose that interfacial sites created by these locally ordered phases that form within amorphous domains can lead to hole-ion separation with a similar mechanism as the one reported by Zhong et al. for nanocrystalline P3HT films.[55]

Now, we discuss the differences seen in the slow decay components of the TA kinetics that reflect populations of trapped polarons (see region labeled "B" in Figure 5b). The TA kinetics during the 1–100 ps timescale decay faster for the doped (100:0) polymer film compared to the doped (50:50) polymer film. We quantified these differences empirically using a sum of two stretched exponentials to fit the TA kinetic data:

$$f(t) = N\left(w_1 e^{\left(-t/\tau_1\right)^{\beta_1}} + w_2 e^{\left(-t/\tau_1\right)^{\beta_2}}\right) \quad (1)$$

where τ_1 and τ_2 are the Williams-Watts time constants for each stretched exponential, β_1 and β_2 are the Williams-Watts stretching parameters, w_1 and w_2 are weighting coefficients that satisfy both $0 \leq w_1, w_2 \leq 1$ and $w_2 = 1 - w_1$, and N is a normalization constant that scales the entire function. This function (Equation (1)) was convoluted with a Gaussian function representing the instrument response function (IRF) before fitting the data using nonlinear least squares (see Figure S5, Supporting Information). The resulting fits are overlaid on the kinetic data (black lines in Figure 5b) and show excellent agreement. Stretched exponentials were chosen over other functions, such as exponentials, to appropriately describe the dispersion seen in the decay kinetics. Additional details on the fitting procedure and on the theory of the stretched exponential function are provided in the Supporting Information.

The stretched exponential function reveals information about the distribution of relaxation times arising due to heterogeneity from a superposition of numerous exponential decay functions.[63] The relaxation time (Williams–Watts, WW) distribution function $G_{\mathrm{WW}}(\tau)$, which is calculated using the Williams–Watts time constant τ_{WW} and stretching parameter β_{WW}, is a convenient way for qualitatively visualizing dispersion in relaxation time. The first moment of the distribution function, which is called the "average relaxation time" $\langle\tau\rangle_{\mathrm{WW}}$, is also calculated using these two parameters. Figure 5c shows the calculated relaxation time distribution functions for each kinetic decay component for each polymer film. The $\langle\tau\rangle_{\mathrm{WW}}$ values are indicated in Figure 5b next to each kinetic decay component and are tabulated along with all other fit parameters in the Supporting Information. Mobile polarons (fast decay components) have matching relaxation time distribution functions and average relaxation times (i.e., $\langle\tau\rangle_{\mathrm{WW}} \approx 0.1$ ps) for both films, whereas the trapped polarons (slow decay components) show significant differences; the average trapped polaron relaxation time is ≈3 times longer in the (50:50) film than in the (100:0) film, which reflects the skew in the relaxation time distribution function to larger τ_{WW} values.

The WW distribution functions plotted in the right panel of Figure 5c provide an alternative way to visualize the differences between the average relaxation time of trapped polarons in the (100:0) and (50:50) films. These distribution functions, which are plotted against WW time constant τ_{WW}, show the distribution of relaxation times of each population of excited polarons. The WW distribution function of the (50:50) film (blue trace in the right panel of Figure 5c) is more shifted toward longer time constants, signifying that the photoexcited polarons in this film have longer relaxation times on average.

Morphological differences in the P3HT phases in each film reveal why the trapped polaron population decays more slowly for the (50:50) film. In disordered materials like organic polymers, carriers transport via thermally-activated hopping from one localized state to another within a density of states that is determined by energetic disorder.[64–68] Because the excitation pulse in TA spectroscopy photoseparates the hole from the counterion, the decay kinetics reflect the diffusion of the polaron back to the counterion. Therefore, we conclude that a longer average relaxation time seen in the (50:50) film results from polaron diffusion through a broader or deeper distribution of states created by greater disorder in the polymer chains than in the (100:0) film. Although doping improves local ordering of P3HT chains in the (50:50) polymer film, polarons in amorphous, mixed P3HT:F8BT phases trap more deeply on average due to disruption by the F8BT chains. We posit that in this phase, F8BT prevents P3HT chain planarity, which allows the counterion to sit closer to the hole in these P3HT chains, thus preventing hole delocalization.[28]

3. Conclusion

A systematic spectroscopic investigation of the influence of polymer morphology on the dynamics of photoexcited hole polarons is presented. Absorbance spectrophotometry and GI-XRD results showed that blending regioregular P3HT with F8BT hinders the crystallization of P3HT chains in thin films. Sequentially doping a polymer film containing 100% regioregular P3HT (100:0) and a blend P3HT:F8BT film (50:50) results in comparable polaronic signatures in their ground-state absorption spectra, evidencing the generation polarons with similar electronic properties despite differences in their locations within the polymer nanostructure. However, ultrafast transient absorption spectroscopy measurements showed differences in the transient spectra and dynamics of photoexcited polarons, revealing how the P3HT morphology and chain ordering influence the trapping of charge carriers.

Optically exciting the polarons in each polymer film produces a broad photoinduced absorption signal in the near-infrared spectrum that was found to contain overlapping peaks with dispersive decay kinetics that reflect a distribution of mobile (free) and trapped polarons. The peak area kinetics showed biphasic decay for both doped polymer films, indicating the presence of mobile and trapped polarons despite significant differences in their morphologies. The mobile polarons had matching average relaxation times (≈0.1 ps) for both films, whereas the trapped polarons had a three-fold longer average relaxation time for the (50:50) film. The observation of mobile polarons in the amorphous (50:50) film indicates that crystallization is not a requirement for their formation. GI-XRD results of the doped (50:50) polymer film showed evidence of local doping-induced ordering, suggesting that planarization or aggregation is sufficient for the formation of mobile polarons. Observation of a three-fold longer average relaxation time for the trapped polarons in the (50:50) film revealed a deeper distribution of localized states in mixed

P3HT:F8BT phases, in which F8BT prevents local ordering (planarization or aggregation) of the P3HT chains. Altogether, our results indicate that crystallinity is not a requirement for formation of mobile polarons and that local polymer chain ordering is a key design parameter for improving hole transport in conducting polymers. This study further demonstrates transient absorption spectroscopy with direct polaron photoexcitation as a powerful approach for studying the polaron distribution in conducting polymers.

4. Experimental Section

Sample Preparation: A polymer solution of regioregular P3HT (4002-EE, Rieke Metals, M_w ≈50–70 K via GPC, regioregularity > = 90%) was prepared by dissolving ≈20 mg of the powdered polymer in 1 mL chlorobenzene (Mallinckrodt Chemicals). Then, 100 µL of the P3HT polymer solution was diluted with 100 µL of chlorobenzene, and the resulting solution was spin-coated at 800 rpm for 30 s onto a circular 1″ diameter CaF_2 substrate or a 1″ x1″ square glass substrate that were pre-cleaned separately with acetone, isopropanol (IPA), and distilled water in a sonicator bath. The obtained polymer film was then heated on a hotplate for 10 min at 150 °C. A second polymer film was also prepared by diluting 100 µL of the P3HT solution with 100 µL of a chlorobenzene solution containing ≈20 mg of F8BT polymer (Aldrich, average M_w > 20 000). This blended polymer solution was spin-coated onto a pre-cleaned CaF_2 or glass substrate at 800 rpm for 30 s, and the resulting film was allowed to dry without heating. After optical and x-ray measurements of these pristine films, the same films were then doped with an n-butyl acetate solution containing 0.05 mg mL^{-1} $Fe(ClO_4)_3$ (Sigma–Aldrich) via solution sequential processing.[69] The polymer film with 100% P3HT (100:0) was doped by fully covering the film's surface with the dopant solution for 2 min. On the other hand, the dopant solution was allowed to sit on the surface of the blended polymer film (50:50) for 4.33 min. After this doping process, the excess dopant solution was spun off the film at 1000 rpm for 20 s. CaF_2 substrates were used for all-optical spectroscopy measurements, while glass substrates were used for X-ray diffraction measurements.

Steady-State Absorption Spectroscopy: The ground state absorption spectra of the polymer films in the visible and near-infrared regions (400–2500 nm, or 0.5–3.1 eV) were measured using a homebuilt absorbance spectrophotometer as detailed in the previous study.[33] The mid-infrared absorption spectrum of each film was recorded over the 1000–4100 cm^{-1} (0.12–0.51 eV) region using an FT/IR-4X Fourier-transform infrared (FTIR) spectrometer (JASCO) set to 2 cm^{-1} resolution. All steady-state absorption measurements were performed in the transmission geometry.

Grazing-Incidence X-Ray Diffraction: Grazing-incidence X-ray diffraction (GI-XRD) measurements were performed using a SmartLab X-ray diffractometer (Rigaku) using Cu K_α radiation and at a fixed 0.5° angle of incidence. The 2Θ range was scanned from 3°–20°. Vertical and horizontal slits were adjusted so that the incident X-ray beam spot at the sample position was small enough so that the edges of the film samples were not detected. The diffraction patterns were averaged over four separate scans for each sample.

Ultrafast Transient Absorption Spectroscopy: Broadband transient absorption spectroscopy was performed using two different homebuilt ultrafast pump-probe spectrometers, one with spectral sensitivity in the ≈1.24–2.48 eV region (i.e., visible/near-IR) and the other with spectral sensitivity in the ≈0.53–1.38 eV region (i.e., near-IR and short-wave IR (SWIR) regions). Extensive details on the instrument setups are reported elsewhere.[33,70] The doped P3HT (100:0) and doped P3HT:F8BT (50:50) polymer films were optically excited using 0.62 eV (2000 nm) light with excitation fluences of 160 and 132 µJ cm^{-2}, respectively. The fluences were chosen to account for slight differences in film absorption such that the absorbed photon density was ≈4.0×10^{14} cm^{-2}. Due to experimental imperfections in matching the excitation fluence used in each of the TA setups, the near-IR TA spectra were scaled by ≈10% for both samples. For all measurements, a pump (probe) pulse repetition rate of 2.5 kHz (5 kHz) was used, and the TA signals were detected at the magic angle pump-probe geometry.

Supporting Information

Supporting Information is available from the Wiley Online Library or from the author.

Acknowledgements

This work was supported by startup funding from Auburn University and a starter grant award from the Spectroscopy Society of Pittsburgh. X-ray diffraction measurements were performed on a system supported by the NSF Major Research Instrumentation (MRI) program under award number DMR-2018794.

Conflict of Interest

The authors declare no conflict of interest.

Data Availability Statement

The data that support the findings of this study are available from the corresponding author upon reasonable request.

Keywords

conducting polymers, polarons, transient absorption spectroscopy

Received: April 26, 2024
Revised: June 3, 2024
Published online:

[1] S. Logothetidis, *Mater. Sci. Eng. B* **2008**, *152*, 96.
[2] J. Rivnay, R. M. Owens, G. G. Malliaras, *Chem. Mater.* **2014**, *26*, 679.
[3] T. Nguyen-Dang, S. Chae, K. Harrison, L. C. Llanes, A. Yi, H. J. Kim, S. Biswas, Y. Visell, G. C. Bazan, T.-Q. Nguyen, *ACS Appl. Mater. Interfaces* **2022**, *14*, 12469.
[4] S. Inal, G. G. Malliaras, J. Rivnay, *J. Mater. Chem. C* **2016**, *4*, 3942.
[5] S. C. Rasmussen, *ChemPlusChem* **2020**, *85*, 1412.
[6] B. D. Paulsen, S. Fabiano, J. Rivnay, *Annu. Rev. Mater. Res.* **2021**, *51*, 73.
[7] M. Moser, J. F. Ponder, A. Wadsworth, A. Giovannitti, I. McCulloch, *Adv. Funct. Mater.* **2019**, *29*, 1807033.
[8] B. D. Paulsen, K. Tybrandt, E. Stavrinidou, J. Rivnay, *Nat. Mater.* **2020**, *19*, 13.
[9] S. Inal, G. G. Malliaras, J. Rivnay, *Nat. Commun.* **2017**, *8*, 1767.
[10] G. Milczarek, O. Inganäs, *Science* **2012**, *335*, 1468.
[11] J. Rivnay, S. Inal, A. Salleo, R. M. Owens, M. Berggren, G. G. Malliaras, *Nat. Rev. Mater.* **2018**, *3*, 17086.
[12] B. D. Paulsen, R. Wu, C. J. Takacs, H. G. Steinrück, J. Strzalka, Q. Zhang, M. F. Toney, J. Rivnay, *Adv. Mater.* **2020**, *32*, 2003404.
[13] C. Cendra, A. Giovannitti, A. Savva, V. Venkatraman, I. McCulloch, A. Salleo, S. Inal, J. Rivnay, *Adv. Funct. Mater.* **2019**, *29*, 1807034.
[14] J. Tang, Y. Pai, Z. Liang, *ACS Energy Lett.* **2022**, *7*, 4299.
[15] Y. Furukawa, *Synth. Met.* **1995**, *69*, 629.
[16] Y. Shimoi, S. Abe, *Phys. Rev. B* **1994**, *50*, 14781.

[17] A. D. Scaccabarozzi, A. Basu, F. Aniés, J. Liu, O. Zapata-Arteaga, R. Warren, Y. Firdaus, M. I. Nugraha, Y. Lin, M. Campoy-Quiles, N. Koch, C. Müller, L. Tsetseris, M. Heeney, T. D. Anthopoulos, *Chem. Rev.* **2021**, *122*, 4420.
[18] D. A. Stan, Y. Wu, S. H. Tolbert, B. J. Schwartz, *Chem. Mater.* **2021**, *33*, 2343.
[19] D. T. Scholes, P. Y. Yee, G. R. Mckeown, S. Li, H. Kang, R. Lindemuth, X. Xia, S. C. King, D. S. Seferos, S. H. Tolbert, B. J. Schwartz, *Chem. Mater.* **2019**, *31*, 73.
[20] D. T. Scholes, S. A. Hawks, P. Y. Yee, H. Wu, R. Lindemuth, S. H. Tolbert, B. J. Schwartz, *J. Phys. Chem. Lett.* **2015**, *6*, 4786.
[21] D. T. Duong, C. Wang, E. Antono, M. F. Toney, A. Salleo, *Org. Electron.* **2013**, *14*, 1330.
[22] P. Pingel, D. Neher, *Phys. Rev. B* **2013**, *87*, 115209.
[23] R. Ghosh, A. R. Chew, J. Onorato, V. Pakhnyuk, C. K. Luscombe, A. Salleo, F. C. Spano, *J. Phys. Chem. C* **2018**, *122*, 18048.
[24] E. F. Aziz, A. Vollmer, S. Eisebitt, W. Eberhardt, P. Pingel, D. Neher, N. Koch, *Adv. Mater.* **2007**, *19*, 3257.
[25] J. Gao, E. T. Niles, J. K. Grey, *J. Phys. Chem. Lett.* **2013**, *4*, 2953.
[26] J. Gao, B. W. Stein, A. K. Thomas, J. A. Garcia, J. Yang, M. L. Kirk, J. K. Grey, *J. Phys. Chem. C* **2015**, *119*, 16396.
[27] M. T. Fontana, D. A. Stanfield, D. T. Scholes, K. J. Winchell, S. H. Tolbert, B. J. Schwartz, *J. Phys. Chem. C* **2019**, *123*, 22711.
[28] D. T. Scholes, P. Y. Yee, J. R. Lindemuth, H. Kang, J. Onorato, R. Ghosh, C. K. Luscombe, F. C. Spano, S. H. Tolbert, B. J. Schwartz, *Adv. Funct. Mater.* **2017**, *27*, 1702654.
[29] A. R. Chew, R. Ghosh, Z. Shang, F. C. Spano, A. Salleo, *J. Phys. Chem. Lett.* **2017**, *8*, 4974.
[30] R. Noriega, J. Rivnay, K. Vandewal, F. P. V. Koch, N. Stingelin, P. Smith, M. F. Toney, A. Salleo, *Nat. Mater.* **2013**, *12*, 1038.
[31] X. Zhang, H. Bronstein, A. J. Kronemeijer, J. Smith, Y. Kim, R. J. Kline, L. J. Richter, T. D. Anthopoulos, H. Sirringhaus, K. Song, M. Heeney, W. Zhang, I. McCulloch, D. M. DeLongchamp, *Nat. Commun.* **2013**, *4*, 2238.
[32] R. A. Street, *Science* **2013**, *341*, 1072.
[33] A. R. Umar, A. L. Dorris, N. M. Kotadiya, N. C. Giebink, G. S. Collier, C. Grieco, *J. Phys. Chem. C* **2023**, *127*, 9498.
[34] M. G. Voss, D. T. Scholes, J. R. Challa, B. J. Schwartz, *Faraday Discuss.* **2019**, *216*, 339.
[35] L. Wu, S. Casado, B. Romero, J. M. Otón, J. Morgado, C. Müller, R. Xia, J. Cabanillas-Gonzalez, *Macromolecules* **2015**, *48*, 8765.
[36] A. I. Hofmann, R. Kroon, S. Zokaei, E. Järsvall, C. Malacrida, S. Ludwigs, T. Biskup, C. Müller, *Adv. Electron. Mater.* **2020**, *6*, 2000249.
[37] K. Hashimoto, T. Koganezawa, K. Tajima, *J. Am. Chem. Soc.* **2013**, *135*, 9644.
[38] Y. Kim, S. Cook, S. A. Choulis, J. Nelson, J. R. Durrant, D. D. C. Bradley, *Chem. Mater.* **2004**, *16*, 4812.
[39] Y. Kim, D. D. C. Bradley, *Curr. Appl. Phys.* **2005**, *5*, 222.
[40] S. Wood, J. S. Kim, D. T. James, W. C. Tsoi, C. E. Murphy, J.-S. Kim, *J. Chem. Phys.* **2013**, *139*, 064901.
[41] C. R. McNeill, A. Abrusci, I. Hwang, M. A. Ruderer, P. Müller-Buschbaum, N. C. Greenham, *Adv. Funct. Mater.* **2009**, *19*, 3103.
[42] T.-A. Chen, X. Wu, R. D. Rieke, *J. Am. Chem. Soc.* **1995**, *117*, 233.
[43] Y. D. Park, H. S. Lee, Y. J. Choi, D. Kwak, J. H. Cho, S. Lee, K. Cho, *Adv. Funct. Mater.* **2009**, *19*, 1200.
[44] C. Scharsich, R. H. Lohwasser, M. Sommer, U. Asawapirom, U. Scherf, M. Thelakkat, D. Neher, A. Köhler, *J. Polym. Sci., Part B: Polym. Phys.* **2012**, *50*, 442.
[45] P. Y. Yee, D. T. Scholes, B. J. Schwartz, S. H. Tolbert, *J. Phys. Chem. Lett.* **2019**, *10*, 4929.
[46] A. Hamidi-Sakr, L. Biniek, J. Bantignies, D. Maurin, L. Herrmann, N. Leclerc, P. Lévêque, V. Vijayakumar, N. Zimmermann, M. Brinkmann, *Adv. Funct. Mater.* **2017**, *27*, 1700173.
[47] B. Neelamraju, K. E. Watts, J. E. Pemberton, E. L. Ratcliff, *J. Phys. Chem. Lett.* **2018**, *9*, 6871.
[48] E. Lim, A. M. Glaudell, R. Miller, M. L. Chabinyc, *Adv. Electron. Mater.* **2019**, *5*, 1800915.
[49] R. Ghosh, C. M. Pochas, F. C. Spano, *J. Phys. Chem. C* **2016**, *120*, 11394.
[50] I. E. Jacobs, E. W. Aasen, J. L. Oliveira, T. N. Fonseca, J. D. Roehling, J. Li, G. Zhang, M. P. Augustine, M. Mascal, A. J. Moulé, *J. Mater. Chem. C* **2016**, *4*, 3454.
[51] X. M. Jiang, R. Österbacka, O. Korovyanko, C. P. An, B. Horovitz, R. A. J. Janssen, Z. V. Vardeny, *Adv. Funct. Mater.* **2002**, *12*, 587.
[52] J. C. Aguirre, S. A. Hawks, A. S. Ferreira, P. Yee, S. Subramaniyan, S. A. Jenekhe, S. H. Tolbert, B. J. Schwartz, *Adv. Energy Mater.* **2015**, *5*, 1402020.
[53] R. Österbacka, C. P. An, X. M. Jiang, Z. V. Vardeny, *Science* **2000**, *287*, 839.
[54] E. C. Wu, B. J. Schwartz, *J. Chem. Theory Comput.* **2023**, *19*, 6761.
[55] Y. Zhong, V. Untilova, D. Muller, S. Guchait, C. Kiefer, L. Herrmann, N. Zimmermann, M. Brosset, T. Heiser, M. Brinkmann, *Adv. Funct. Mater.* **2022**, *32*, 2202075.
[56] S. Oh, P. H. Nguyen, T. M. Tran, A. J. DeStefano, K. Tagami, D. Yuan, A. Nikolaev, M. Condarcure, S. Han, J. Read De Alaniz, M. L. Chabinyc, *J. Mater. Chem. C* **2023**, *11*, 15435.
[57] L. Sebastian, G. Weiser, H. Bässler, *Chem. Phys.* **1981**, *61*, 125.
[58] J. S. Huff, K. M. Duncan, C. J. Van Galen, M. S. Barclay, W. B. Knowlton, B. Yurke, P. H. Davis, D. B. Turner, R. J. Stanley, R. D. Pensack, *Rev. Sci. Instrum.* **2023**, *94*, 094103.
[59] V. I. Arkhipov, E. V. Emelianova, P. Heremans, H. Bässler, *Phys. Rev. B* **2005**, *72*, 235202.
[60] S. L. Pittelli, S. A. Gregory, J. F. Ponder, S. K. Yee, J. R. Reynolds, *J. Mater. Chem. C* **2020**, *8*, 7463.
[61] T. J. Aubry, K. J. Winchell, C. Z. Salamat, V. M. Basile, J. R. Lindemuth, J. M. Stauber, J. C. Axtell, R. M. Kubena, M. D. Phan, M. J. Bird, A. M. Spokoyny, S. H. Tolbert, B. J. Schwartz, *Adv. Funct. Mater.* **2020**, *30*, 2001800.
[62] E. T. Niles, J. D. Roehling, H. Yamagata, A. J. Wise, F. C. Spano, A. J. Moulé, J. K. Grey, *J. Phys. Chem. Lett.* **2012**, *3*, 259.
[63] C. P. Lindsey, G. D. Patterson, *J. Chem. Phys.* **1980**, *73*, 3348.
[64] V. I. Arkhipov, E. V. Emelianova, G. J. Adriaenssens, *Phys. Rev. B* **2001**, *64*, 125125.
[65] E. V. Emelianova, M. Van Der Auweraer, H. Bässler, *J. Chem. Phys.* **2008**, *128*, 224709.
[66] L. Dou, Y. Liu, Z. Hong, G. Li, Y. Yang, *Chem. Rev.* **2015**, *115*, 12633.
[67] J. Bakalis, A. R. Cook, S. Asaoka, M. Forster, U. Scherf, J. R. Miller, *J. Phys. Chem. C* **2014**, *118*, 114.
[68] M. E. Köse, E. Köse, *Int. J. Quantum Chem.* **2023**, *123*, e27088.
[69] D. T. Scholes, S. A. Hawks, P. Y. Yee, H. Wu, J. R. Lindemuth, S. H. Tolbert, B. J. Schwartz, *J. Phys. Chem. Lett.* **2015**, *6*, 4786.
[70] A. L. Dorris, A. R. Umar, C. Grieco, *Appl. Spectrosc.* **2024**, https://doi.org/10.1177/00037028241247072.